Graphene woven fabric-reinforced polyimide films with enhanced and anisotropic thermal conductivity

Jinrui Gong [a,b,1], Zhiduo Liu [b,1], Jinhong Yu [b,*], Dan Dai [b], Wen Dai [b], Shiyu Du [c], Chaoyang Li [d], Nan Jiang [b], Zhaolin Zhan [a,*], Cheng-Te Lin [b,*]

[a] Faculty of Materials Science and Engineering, Kunming University of Science and Technology, Kunming 650093, China
[b] Key Laboratory of Marine Materials and Related Technologies, Zhejiang Key Laboratory of Marine Materials and Protective Technologies, Ningbo Institute of Materials Technology and Engineering, Chinese Academy of Sciences, Ningbo 315201, China
[c] Division of Functional Materials and Nanodevices, Ningbo Institute of Materials Technology and Engineering, Chinese Academy of Sciences, Ningbo, Zhejiang 315201, China
[d] Research Institute & School of Systems Engineering, Kochi University of Technology, Kami City, Kochi 782-8502, Japan

A B S T R A C T

Due to the growing needs of thermal management in modern electronics, polyimide-based (PI) composites are increasingly demanded in thermal interface materials (TIMs). Graphene woven fabrics (GWFs) with a mesh structure have been prepared by chemical vapor deposition and used as thermally conductive filler. With the incorporation of 10-layer GWFs laminates (approximate 12 wt%), the in-plane thermal conductivity of GWFs/PI composite films achieves 3.73 W/mK, with a thermal conductivity enhancement of 1418% compared to neat PI. However, the out-of-plane thermal conductivity of the composites is only 0.41 W/mK. The in-plane thermal conductivity exceeds its out-of plane counterpart by over 9 times, indicating a highly anisotropic thermal conduction of GWFs/PI composites. The thermal anisotropy and the enhanced in-plane thermal conductivity can be attributed to the layer-by-layer stacked GWFs network in PI matrix. Thus, the GWFs-reinforced polyimide films are promising for use as an efficient heat spreader for electronic cooling applications.

Keywords:
A. Graphene
A. Polymer-matrix composites (PMCs)
A. Thermosetting resin
B. Thermal properties

1. Introduction

Polymer-based composites have diverse applications in automobile, aerospace and electronics industries, due to their low-cost, light weight, recyclability, good process ability, and enhanced physical properties compared to the polymer itself. Especially, in recent years, on account of the growing requirements of high density and speed circuits in electronic equipment, the efficient dissipation of heat generated by electronic components has caused considerable attention to avoid thermal damage to the system. In order to solve this issue, great efforts have been dedicated to improve the heat conduction performance of polymer composites [1–3].

Graphene, a one-atom-thick layer of sp^2-bonded carbon atoms [4], has been extensively studied for various applications in the recent decade [5–7], based on its ultrafast electron mobility [8], excellent mechanical strength [9], and extremely high specific surface area [10]. Besides, due to the extraordinary thermal conductivity, graphene and its derivatives have been recognized as promising fillers to fabricate polymer-matrix composites for thermal management applications [2,11]. In theory, the thermal conductivity of perfect graphene could be up to 5300 W/mK, which is three times higher than diamond [12]. In the past few years, a variety of graphene related materials were reported to be incorporated with the polymer matrix for improving the thermal properties, such as graphene nanoplatelets [13–15], graphene nanosheets [16,17], and graphene oxide [18–20]. However, the reinforcing effect on the composites is still limited because of the defects of graphene, weak interfacial interaction and poor dispersion of graphene in the polymer matrix.

In contrast to commonly used methods to homogeneously disperse graphene fillers in the matrix, more recently, graphene with three-dimensional (3D) interconnected structure has gained much attention for fabrication of nanocomposites [21]. 3D graphene network has many advantages, such as relatively large surface area with a low density, and the formation of continuous thermal and electrical conduction paths [22]. Currently, 3D graphene structure was prepared by using self-assembly techniques like hydrothermal [23] or sol–gel methods [24], followed by freeze-drying or super

* Corresponding authors.
E-mail addresses: yujinhong@nimte.ac.cn (J. Yu), zl_zhan@sohu.com (Z. Zhan), linzhengde@nimte.ac.cn (C.-T. Lin).

critical treatments [25–27]. Alternatively, 3D graphene network can be also prepared by chemical vapor deposition (CVD) method, which enables to grow graphene on Ni and Cu foams [28,29] or meshes [30,31] as catalyst templates. Compared to those graphene derivatives made by exfoliation of graphite, CVD-grown graphene has less defects and superior thermal and mechanical properties. For example, Jia et al. reported that exceptionally high electrical conductivity of epoxy composites can be achieved by infiltrating epoxy into 3D interconnected graphene, which was grown by CVD on Ni foam [29]. However, there have been only a few works on thermally conductive polymer composites by incorporation of CVD-derived 3D graphene structure [21].

To be a matrix, polyimide (PI) has been widely investigated due to its high thermal stability, good mechanical properties and low dielectric constant [18,32,33]. However, the thermal conductivity of PI matrix is the order of 0.1 W/mK at room temperature [34], which cannot meet the heat dissipation requirements of modern electronic components and electrical systems. The low thermal conductivity of PI is attributed to the random orientation of molecular chains in amorphous PI region, leading to the reduction of the mean free path of heat conducting phonons [35,36]. The addition of high thermally conductive fillers in the PI matrix is helpful to overcome this drawback. But, to avoid the deterioration of other properties, it still presents a challenge to achieve a balance of high thermal conductivity and low filler content for fabricating PI composites.

In this study, we developed a PI composite incorporated with 3D graphene structure, which was constructed by lamination of graphene woven fabrics (GWFs). GWFs were fabricated by CVD growth of graphene layers on Ni woven fabrics. As a result, the incorporation of GWFs in the PI matrix shows a significant enhancement of thermal conductivity, especially along the in-plane direction. The GWFs/PI composite films are promising for using as a heat dissipation material.

2. Experimental

2.1. Materials

Ni mesh (200 mesh; purity: 99.9%) was purchased from Hebei Hang Xu Co., Ltd, China. The mesh is woven with the yarn of 45 μm in diameter and the grid size is 70 × 70 μm. Poly(amic acid) (PAA) synthesized by pyromellitic dianhydride and 4,4′-oxydianiline was obtained from Ningbo Cen Electrical Material Co., Ltd, China. N,N'-dimethyl acetamide (DMAc) were purchased from Sinopharm Chemical Reagent Co., Ltd, China. All chemicals were of analytical reagent grade and used without further purification.

2.2. Preparation of GWFs

CVD method was employed to grow graphene layers on the Ni surface, which was commonly used as a catalyst template for preparation of few-layer graphene [21,28,29]. Accordingly, GWFs with a similar structure of Ni mesh could be prepared by CVD, as follows: Ni mesh was first sonicated in acetic acid solution to remove the impurities and surface oxides. The mesh was then placed in a quartz tube furnace, followed by the rise of the furnace temperature at the heating rate of 10 °C/min with the H_2 flow (8 sccm). As the temperature reached 1000 °C, the system was kept for 15 min for annealing of Ni mesh. A mixture of CH_4 (24 sccm) and H_2 (8 sccm) was then introduced into the tube furnace for the catalytic growth of graphene. After reaction for 30 min, the sample was cooled down rapidly at the cooling rate of 200 °C/min. GWFs could be obtained after removal of Ni in the etching solution (10 g $CuSO_4$ and 50 ml HCl in 50 ml DI water).

2.3. Fabrication of GWFs/PI composites

To fabricate GWFs/PI composite films, 3D graphene structure was first prepared by layer-by-layer stacking of GWFs. 10-layer laminate of GWFs was then impregnated by PAA solution (dissolved in DMAc), followed by degassing in vacuum. The as-prepared sample was baked in a vacuum furnace at 80 °C for 2 h and at 120, 150, 200, 250, 300, and 350 °C for 1 h, respectively, to complete imidization reaction. The experimental process is schematically illustrated in Fig. 1.

2.4. Characterization

Raman spectra were obtained by Raman spectrometer with laser wavelength of 532 nm (Renishaw plc, Wotton-under-Edge, UK). X-ray photoelectron spectroscopy (XPS) was carried out with Kratos AXIS ULTR DLD spectrometer. Fourier transform infrared (FTIR) spectra were obtained using a Nicolet 6700 FTIR (Thermal scientific Inc. USA) between 400 and 4000 cm^{-1}. The morphology and microstructure of GWFs and the composites were examined by optical microscope (OM, Leica DM 2500 M, Germany) and scanning electron microscopy (SEM, Quanta FEG250, USA) equipped with energy dispersive spectroscopy (EDS), and transmission electron microscopy (TEM, JEOL JEM-2100, Japan), respectively. Thermal conductivities of the composites were characterized with laser flash apparatus (LFA, NETZSCH 447, Germany) at room temperature. The sample for in-plane and out-of plane measurement was round with a diameter of 25.4 mm and 12.7 mm, respectively. Thermogravimetric analysis (TGA) was carried out using NETZSCH STA-449 thermo-analyzer. The temperature range was from 30 to 900 °C at a heating rate of 10 °C/min in nitrogen. The IR-photos were captured by infrared camera (Fluke, Ti400, USA).

3. Results and discussion

3.1. Characterizations of GWFs

A photograph of Ni mesh, graphene-deposited mesh, and a thin layer of GWFs after Ni etching, respectively, is presented in Fig. 2a. The lateral size of our GWFs can be up to 30 × 50 cm. We found that the color of the samples turned into black from light gray after CVD growth, and then became dark gray after removal of Ni. Fig. 2b shows the typical Raman spectra taken from a single yarn (position A) and the woven joint (position B) in GWFs, respectively. Both spectra exhibit the characteristic peaks of graphene: a sharp G-band (at 1580–1583 cm^{-1}), a strong 2D-band (at 2697–2700 cm^{-1}), and a tiny D-band (at 1351–1358 cm^{-1}) [37]. The origin of G-band is attributed to the stretching-vibration mode of sp^2 sites, and 2D-band is formed of a double-resonance process [37–39]. The weak D-band, based on the bond-angle disorder due to the formation of sp^3 bonds, suggests the high-quality of graphene layers grown by CVD. Moreover, according to Reina's work [40], the intensity ratio from the 2D-band to G-band (I_{2D}/I_G) can be associated with the number of graphene layers. The I_{2D}/I_G ratio at position A is 2.25, which can be assigned to single- to bi-layer graphene [39], however, the spectra of few-layer graphene can be also found (see Fig. S1). At position, B the signal may come from graphene with more layers (I_{2D}/I_G ratio: 1.16) because of the overlapping of two yarns.

XPS analysis is a useful tool to determine the chemical compositions of graphene layers, and able to provide information on the types of oxygen-containing functional groups on the graphene. The

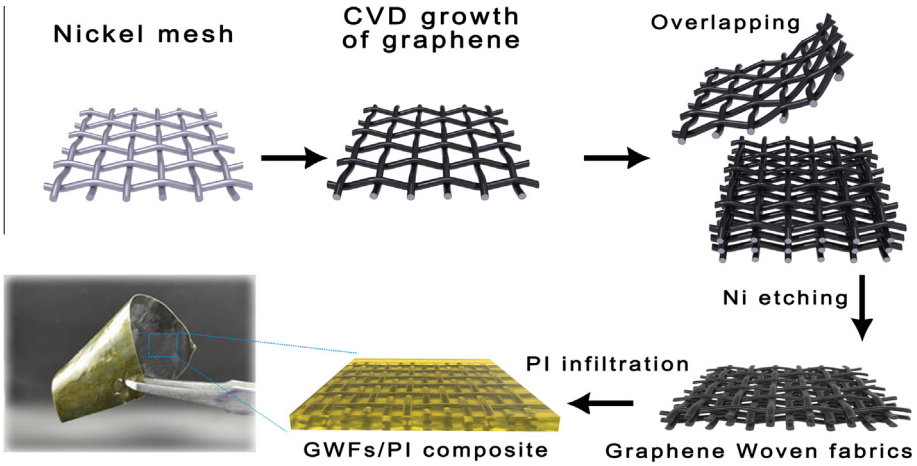

Fig. 1. The schematic illustration of the fabrication process of GWFs/PI composite films. (For interpretation of the references to color in this figure legend, the reader is referred to the web version of this article.)

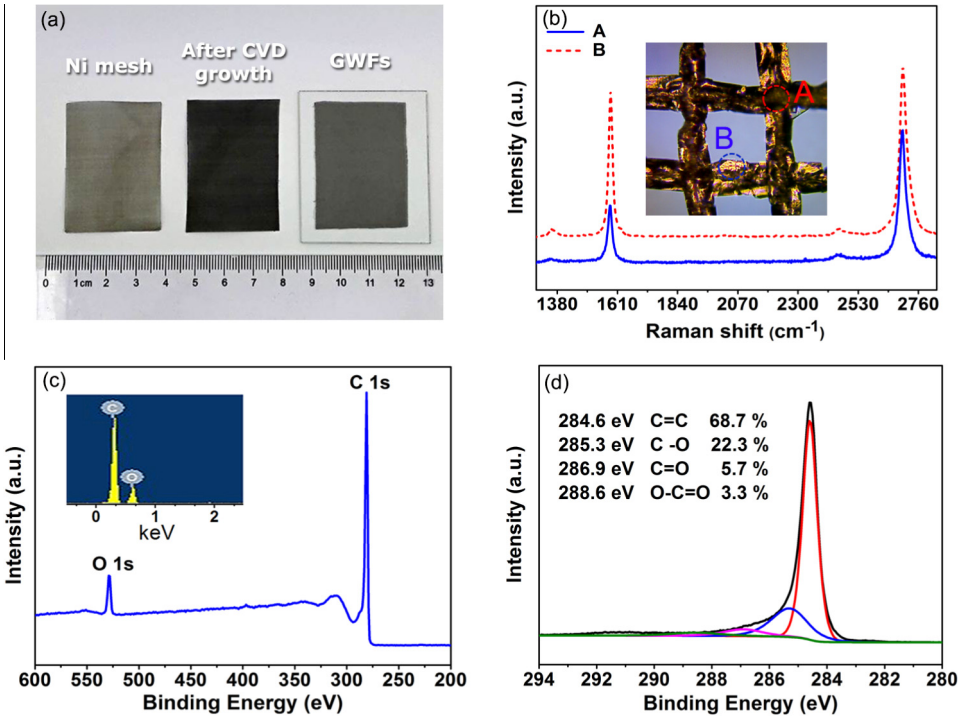

Fig. 2. (a) A photograph showing the preparation process of GWFs, (b) Raman, (c) XPS survey, and (d) XPS C1s spectra of as-prepared GWFs. (For interpretation of the references to color in this figure legend, the reader is referred to the web version of this article.)

XPS spectra in Fig. 2c indicates that GWFs are comprised of carbon and a trace amount of oxygen; the latter may be ascribed to the adsorbed moisture or oxygen onto the surface of graphene. The absence of Ni signal at binding energies of 850–870 eV and in EDS spectrum (the inset of Fig. 2c) suggests that Ni mesh has been completely removed after etching [41]. Furthermore, as a fitting result in Fig. 2d, high-resolution C1s spectrum consists of four components: C=C/C—C (sp^2/sp^3 bonding, 284.6 eV), C—O (hydroxyl group, 285.3 eV), C=O (carbonyl group, 286.9 V), and O—C=O (carboxyl group, 288.6 eV) [42]. It shows that our GWFs contain 68.7% carbons and 31.3% oxygen-containing functional groups.

The observation in TEM (Fig. 3a) shows that a single yarn in GWFs is composed of tubular graphene structure. The characteristic hexagonal diffraction pattern (the right top inset of Fig. 3a) obtained at the edge of few-layer graphene in Fig. 3a suggests high crystalline degree of our samples. As presented in Fig. 3b and c, the wall of the tubular structure mainly consists of single- and bilayer graphene, which is in good agreement with the result of Raman spectra (Fig. 2b).

The use of GWFs as fillers in the polymer composites has an additional advantage when compared to CVD-synthesized graphene films [43–46]. That is, when a stretching force is applied, the characteristic structure of GWFs allows the deformation of GWFs without the formation of cracks or fractures. As presented in Fig. 4a and a GWF layer (approximate 105 μm) was first attached on elastic poly (dimethyl siloxane) (PDMS) substrate,

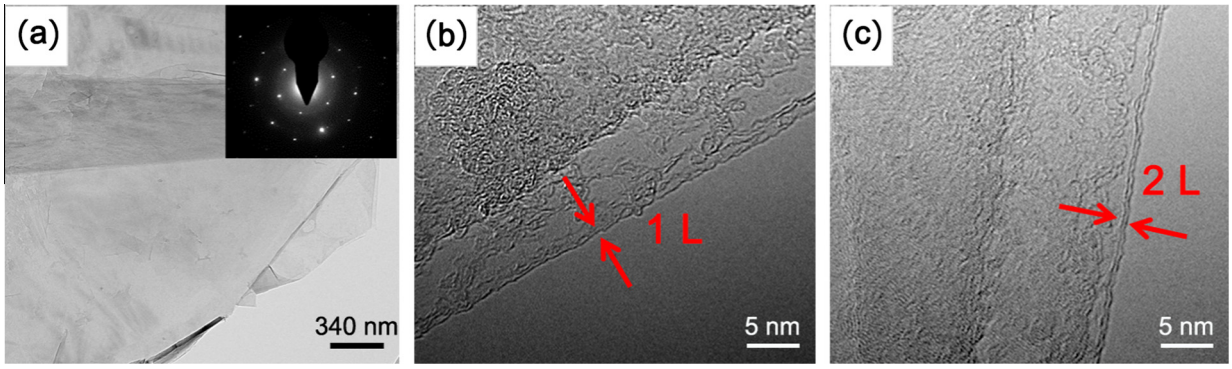

Fig. 3. (a) TEM image and the corresponding diffraction pattern of as-prepared GWFs (right top inset), (b) and (c) high-resolution TEM images of the wall of the tubular structure in GWFs. (For interpretation of the references to color in this figure legend, the reader is referred to the web version of this article.)

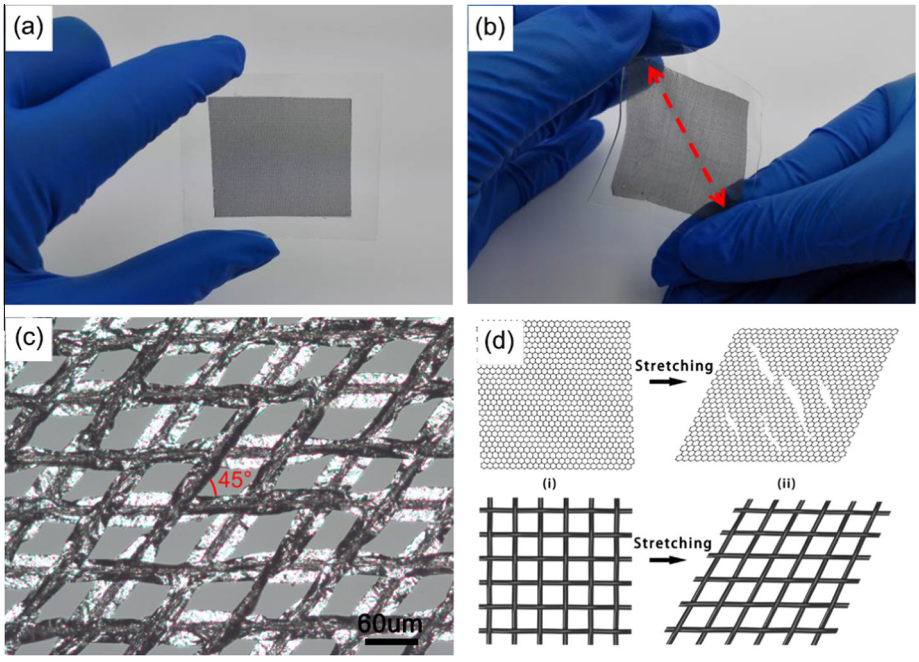

Fig. 4. The photographs of GWFs adhering on the PDMS substrate (a) before and (b) after stretching, (c) OM image of the grids in the stretched GWFs, (d) a scheme illustrating the structure of a graphene film and a GWFs layer after stretching. (For interpretation of the references to color in this figure legend, the reader is referred to the web version of this article.)

and then the GWFs/PDMS sheet was uniaxially stretched at a 45° angle. In the optical microscope (OM) image of Fig. 4c, we noticed that the network structure of GWFs remains after stretching, due the fact that the grids in GWFs could deform accordingly to release the stretching force. In Fig. 4d, a comparative illustration shows the resulting morphology of a graphene film and a GWF layer deformed by applying a stretching force. A lot of cracks would occur on the surface of mechanically stretched graphene film, whereas the network structure of GWFs is not affected.

3.2. The morphology of GWFs and GWFs/PI composites

GWFs/PI composite films were fabricated by impregnation of 10-layer-stacked GWFs in PAA solution, followed by thermal treatment for imidization. The morphological variation of the samples was examined and presented in Fig. 5. Fig. 5a–d show the optical microscope images of pristine Ni mesh, Ni mesh after CVD growth, GWFs and GWFs/PI composites, respectively. As shown in images, GWFs still keep the intact graphene woven fabrics structure in GWFs/PI Composites. In Fig. 5e and i, the Ni mesh exhibits a typical woven structure and a smooth surface. Fig. 5f and j display the SEM images of graphene deposited on the surface of Ni mesh. The Ni surface has been completely covered with graphene layers and the wrinkles of graphene is clearly identified (see Fig. S2) after CVD growth. The formation of graphene on polycrystalline Ni by CVD is based on the non-equilibrium precipitation mechanism of carbon atoms from Ni [47]. In short, during CVD, carbon atoms were generated from the decomposition of CH_4 and then diffused into the Ni. Subsequently, during the rapid cooling process, super saturated carbon atoms inside the Ni would segregate on the Ni surface, leading to the formation of single- to few-layer graphene [48]. After removal of Ni, the obtained GWFs reveal a well-preserved mesh structure, as shown in Fig. 5c. The collapse of graphene yarns (Fig. 5g) and the cross-sectional SEM image of a single yarn (Fig. 5k) demonstrate that GWFs are composed of tubular graphene structure, which allows PAA solution to easily flow into the

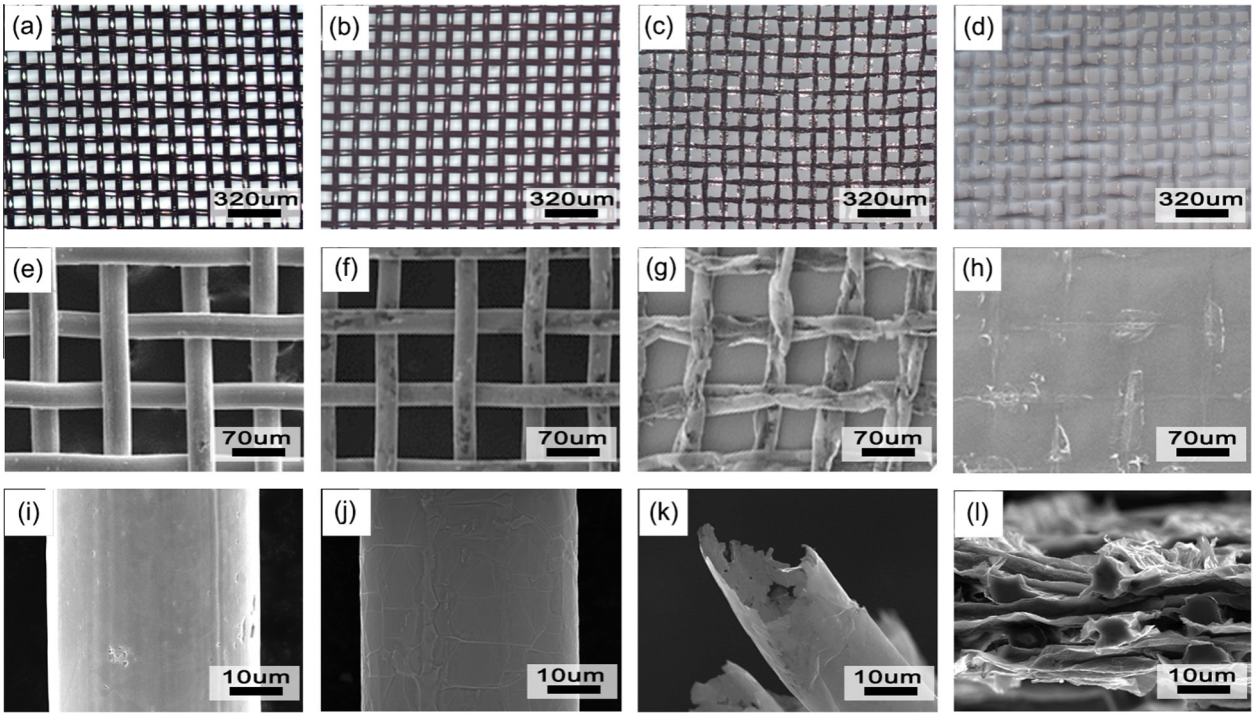

Fig. 5. (a–d) OM, (e–h) SEM, and (i–l) high-magnification SEM images of Ni mesh, graphene-deposited Ni mesh, GWFs, and GWFs/PI composites, respectively.

inside of GWFs. TEM investigation for the microstructure of GWFs confirms the above observations of SEM images, and proves that GWFs mainly consist of single- or bilayer graphene (see Fig. 3). The top-view of GWFs embedded in the PI matrix can be seen in Fig. 5d and h, in addition, the cross-sectional view manifests that GWFs layers have been well incorporated in the PI matrix (Fig. 5l).

3.3. Thermal properties of GWFs/PI composites

The thermal diffusivity and thermal conductivity of GWFs/PI composite films with 12 wt% loading of GWFs along the out-of and in-plane directions, respectively, are shown in Fig. 6a. The thermal properties of neat PI are also exhibited for comparison. The thermal diffusivity (α) of the samples was determined by LFA at room temperature and ambient pressure. The value of thermal conductivity (κ) could be evaluated by the equation: $\kappa = \alpha \times \rho \times C_p$, where α is thermal diffusivity, ρ is the measured density, and C_p is specific heat capacity of the samples [49]. We found that the out-of plane thermal conductivity of GWFs/PI composite films is 0.41 W/mK, which gives a slight improvement (≈66%), compared to that of neat PI (0.25 W/mK). Interestingly, GWFs/PI composite films present the effective thermal conductivity enhancement (TCE) along the in-plane direction, which increases up to 1418%. The value of 3.73 W/mK for the in-plane thermal conductivity of GWFs/PI composite films can be achieved, with the incorporation of 12 wt% GWFs (10-layer GWFs). In addition, the thermal diffusivity and thermal conductivity of GWFs/PI composites containing different GWFs was shown in Fig. S4. It is clear that the thermal diffusivity and thermal conductivity of GWFs/PI composites increases with the incorporation of the GWFs fillers. As a result, we conclude that GWFs/PI composite films show a highly anisotropic thermal property, with a ratio of over 9 times between out-of and in-plane thermal conductivities, which is superior to other anisotropic polymer composites filled with graphene nanoplatelets or nanoribbons [3,50,51]. The highly anisotropic thermal conduction of GWFs/PI composites can be attributed to the particular stacking of GWFs layers in the PI matrix [50,52]. The preferred in-plane direction for heat transport is due to the formation of interconnected planar network of GWFs. In contrast, the interfacial thermal resistance between GWFs laminates is large, resulting in a lower enhancement for the out-of plane conduction. Moreover, compared to other nanofillers-filled PI composites (Table 1), our samples achieve higher thermal conductivity at relatively low filler content, which is because of the associated benefits of high-quality graphene prepared by CVD, and the effective conduction paths based on 3D graphene structure [21,58].

The significant improvement of the in-plane thermal conductivity enables GWFs/PI composite films for use as a heat spreader for electronic cooling applications. To examine the heat dissipation performance of our composite sample, neat PI and GWFs/PI composite strips were separately connected between the heat sink and a heater. The size of each strip is 30.0 (length) × 5.0 (width) × 1.2 mm (thickness). In addition, the temperature profile evolution in time of two samples was recorded using a calibrated infrared (IR) camera. As shown in Fig. 6b, IR images present the temperature increase of neat PI and GWFs/PI composites from one side to another, respectively, as a function of heating time. The temperature of two samples at the position with the same distance from the heater was determined for comparison. Before testing, the whole system was kept at room temperature. As the heater temperature rose, we noticed that the temperature increase of GWFs/PI composites was faster than that of neat PI. When the heater reached 180 °C, the temperature of GWFs/PI composites was 99 °C, which increased by 13 °C than 86 °C of neat PI. This result demonstrates that GWFs-reinforced PI films have better heat dissipation performance in the real case, which is in good agreement with the higher thermal conductivity of GWFs/PI composites along the in-plane direction. Meanwhile, Fig. S5 presents the excellent thermal stability of GWFs/PI composites in comparison with the neat PI.

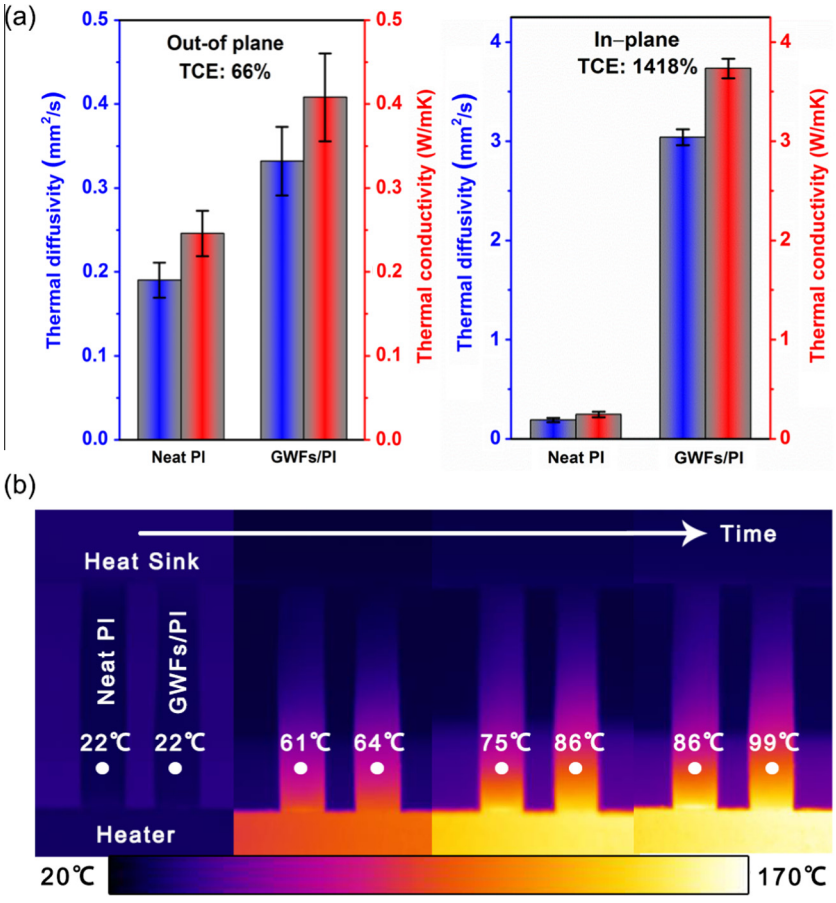

Fig. 6. Thermal properties of GWFs/PI composite films: (a) thermal diffusivity and thermal conductivity of neat PI and GWFs/PI composite along out-of and in-plane directions. (b) IR images displaying the temperature change of neat PI and GWFs/PI composite films as a function of heating time. (For interpretation of the references to color in this figure legend, the reader is referred to the web version of this article.)

Table 1
A comparison of various thermal conductive nanofillers for fabrication of polyimide composites.

Filler types	TCE (%)	Thermal conductivity (W/mK)	Fraction (wt%)
Functionalized BN [53]	562	0.86	50
Graphene sheets [54]	294	1.00	11
ZnO nanoparticles [55]	410	1.54	59
Micro- and nano-sized BN hybrids [34]	500	1.20	30
Graphene oxide [56]	608	0.92	20
Graphene/SiC hybrids [57]	989	2.63	11
GWFs (this work)	1418	3.73	12

4. Conclusions

In this work, the thermally conductive PI composites have been developed with the incorporation of GWFs laminates, which exhibit better stretching allowance than continuous graphene films. The in-plane thermal conductivity of GWFs/PI composite films with 12 wt% GWFs loading is up to 3.73 W/mK, which increased by 1418% of TCE as compared to that of neat PI. In contrast, the out-of plane thermal conductivity of the composites is 0.41 W/mK, with an increase of TCE of only 66%. The thermal anisotropy and the improvement of the in-plane thermal conductivity can be ascribed to the particular stacking of high-quality GWFs in the PI matrix. The excellent thermal properties allow GWFs/PI composite films for use as an efficient heat spreader for thermal management in electronics.

Acknowledgements

The authors are grateful for the financial support by the National Natural Science Foundation of China (Nos. 51303034 and 51573201), Natural Science Foundation of Ningbo (2014A610111), Public Welfare Project of Zhejiang Province (2016C31026) and International Science and Technology Cooperation Program of Ningbo (2015D10003) for financial support. We also thank the Chinese Academy of Science for Hundred Talents Program, Chinese Central Government for Thousand Young Talents Program, and The Key Technology of Nuclear Energy (CAS Interdisciplinary Innovation Team, 2014).

Appendix A. Supplementary material

Supplementary data associated with this article can be found, in the online version, at http://dx.doi.org/10.1016/j.compositesa.2016.05.010.

References

[1] Bozlar M, He D, Bai J, Chalopin Y, Mingo N, Volz S. Carbon nanotube microarchitectures for enhanced thermal conduction at ultralow mass fraction in polymer composites. Adv Mater 2010;22(14):1654–8.
[2] Shahil KMF, Balandin AA. Graphene-multilayer graphene nanocomposites as highly efficient thermal interface materials. Nano Lett 2012;12(2):861–7.
[3] Ding P, Zhuang N, Cui X, Shi L, Song N, Tang S. Enhanced thermal conductive property of polyamide composites by low mass fraction of covalently grafted graphene nanoribbons. J Mater Chem C 2015;3(42):10990–7.

[4] Novoselov1 KS, Geim AK, Morozov SV, Jiang D, Zhang Y, Dubonos SV, et al. Electric field effect in atomically thin carbon films. Science 2004;306(5696):666–9.
[5] Lin CT, Loan PTK, Chen TY, Liu KK, Chen CH, Wei KH, et al. Label-free electrical detection of DNA hybridization on graphene using hall effect measurements: revisiting the sensing mechanism. Adv Funct Mater 2013;23(18):2301–7.
[6] Jung SM, Daniela LM, Lin CT, Jung HY, Kong J. Controlled porous structures of graphene aerogels and their effect on supercapacitor performance. Nanoscale 2015;7(10):4386–93.
[7] Yang T, Wang W, Zhang H, Li X, Shi J, He Y, et al. Tactile sensing system based on arrays of graphene woven microfabrics: electromechanical behavior and electronic skin application. ACS Nano 2015;9(11):10867–75.
[8] Hesjedal T. Continuous roll-to-roll growth of graphene films by chemical vapor deposition. Appl Phys Lett 2011;98(13):133106.
[9] Lee C, Wei X, Kysar JW, James Hone J. Measurement of the elastic properties and intrinsic strength of monolayer graphene. Science 2008;321(5887):385–8.
[10] Chae HK, Siberio-Pérez DY, Kim J, Go YB, Eddaoudi M, Matzger AJ, et al. A route to high surface area, porosity and inclusion of large molecules in crystals. Nature 2004;427(6974):523–7.
[11] Renteria J, Legedza S, Salgado R, Balandin MP, Ramirez S, Saadah M, et al. Magnetically-functionalized self-aligning graphene fillers for high-efficiency thermal management applications. Mater Des 2015;88:214–21.
[12] Balandin AA, Ghosh S, Bao W, Calizo I, Teweldebrhan D, Miao F, et al. Superior thermal conductivity of single-layer graphene. Nano Lett 2008;8(3):902–7.
[13] Gu J, Xie C, Li H, Dang J, Geng W, Zhang Q. Thermal percolation behavior of graphene nanoplatelets/polyphenylene sulfide thermal conductivity composites. Polym Compos 2014;35(6):1087–92.
[14] Guo WM, Chen G. Fabrication of graphene/epoxy resin composites with much enhanced thermal conductivity via ball milling technique. J Appl Polym Sci 2014;131(15).
[15] Le MT, Huang SC. Thermal and mechanical behavior of hybrid polymer nanocomposite reinforced with graphene nanoplatelets. Materials 2015;8(8):5526–36.
[16] Sheng X, Xie D, Cai W, Zhang X, Zhong L, Zhang H. In situ thermal reduction of graphene nanosheets based poly(methyl methacrylate) nanocomposites with effective reinforcements. Ind Eng Chem Res 2015;54(2):649–58.
[17] Yan H, Wang R, Li Y, Long W. Thermal conductivity of magnetically aligned graphene-polymer composites with Fe_3O_4-decorated graphene nanosheets. J Electron Mater 2015;44(2):658–66.
[18] Wang JY, Yang SY, Huang YL, Tien HW, Chin WK, Ma CCM. Preparation and properties of graphene oxide/polyimide composite films with low dielectric constant and ultrahigh strength via in situ polymerization. J Mater Chem 2011;21(35):13569.
[19] Park OK, Kim SG, You BC, Hui D, Lee JH. Synthesis and properties of iodo functionalized graphene oxide/polyimide nanocomposites. Compos B 2014;56:365–71.
[20] Fang X, Liu X, Cui ZK, Qian J, Pan J, Li X, et al. Preparation and properties of thermostable well-functionalized graphene oxide/polyimide composite films with high dielectric constant, low dielectric loss and high strength via in situ polymerization. J Mater Chem A 2015;3(18):10005–12.
[21] Zhao YH, Wu ZK, Bai SL. Study on thermal properties of graphene foam/graphene sheets filled polymer composites. Compos Part A 2015;72:200–6.
[22] Shih MH, Li LJ, Yang YC, Chou HY, Lin CT, Su CY. Efficient heat dissipation of photonic crystal microcavity by mono layer graphene. ACS Nano 2013;7(12):10818–24.
[23] Yu DA, Wei L, Jiang W, Wang H, Sun B, Zhang Q, et al. Nitrogen doped holey graphene as an efficient metal-free multifunctional electrochemical catalyst for hydrazine oxidation and oxygen reduction. Nanoscale 2013;5(8):3457.
[24] Bai H, Li C, Wang X, Shi G. On the gelation of graphene oxide. J Phys Chem C 2011;115(13):5545–51.
[25] Vickery JL, Patil AJ, Mann S. Fabrication of graphene-polymer nanocomposites with higher-order three-dimensional architectures. Adv Mater 2009;21(21):2180–4.
[26] He Y, Zhang N, Gong Q, Li Z, Gao J, Qiu H. Metal nanoparticles supported graphene oxide 3D porous monoliths and their excellent catalytic activity. Mater Chem Phys 2012;134(2–3):585–9.
[27] Sun H, Xu Z, Gao C. Multifunctional, ultra-flyweight, synergistically assembled carbon aerogels. Adv Mater 2013;25(18):2554–60.
[28] Cao X, Shi Y, Shi W, Lu G, Huang X, Yan Q, et al. Preparation of novel 3D graphene networks for supercapacitor applications. Small 2011;7(22):3163–8.
[29] Jia J, Sun X, Lin X, Shen X, Mai YW, Kim JK. Exceptional electrical conductivity and fracture resistance of 3D interconnected graphene foam/epoxy composites. ACS Nano 2014;8(6):5774–83.
[30] Li X, Sun P, Fan L, Zhu M, Wang K, Zhong M, et al. Multifunctional graphene woven fabrics. Sci Rep 2012;4(2):395.
[31] Wang Y, Yang T, Lao J, Zhang R, Zhang Y, Zhu M, et al. Ultra-sensitive graphene strain sensor for sound signal acquisition and recognition. Nano Res 2015;8(5):1627–36.
[32] Chung IS, Park CE, Ree M, Kim SY. Soluble polyimides containing benzimidazole rings for interlevel dielectrics. Chem Mater 2001;13(9):2801–6.
[33] Wu Z, Wu D, Yang W, Jin R. Preparation of highly reflective and conductive metallized polyimide films through surface modification: processing, morphology and properties. J Mater Chem 2006;16(3):310–6.
[34] Li TL, Hsu SLC. Enhanced thermal conductivity of polyimide films via a hybrid of micro- and nano-sized boron nitride. J Phys Chem B 2010;114(20):6825–9.
[35] Hu Y, Shen J, Li N, Ma H, Shi M, Yan B, et al. Comparison of the thermal properties between composites reinforced by raw and amino-functionalized carbon materials. Compos Sci Technol 2010;70(15):2176–82.
[36] Im H, Kim J. Effect of homogeneous $Al(OH)_3$ covered MWCNT addition on the thermal conductivity of Al_2O_3/epoxy-terminated poly(dimethylsiloxane) composites. J Mater Sci 2012;47(16):6025–33.
[37] Gupta A, Chen G, Joshi P, Tadigadapa S, Eklund PC. Raman scattering from high-frequency phonons in supported n-graphene layer films. Nano Lett 2006;6(12):2667–73.
[38] Ferrari AC, Robertson J. Interpretation of Raman spectra of disordered and amorphous carbon. Phys Rev B 2000;61(20):14095–107.
[39] Ferrari AC, Meyer JC, Scardaci V, Casiraghi C, Lazzeri M, Mauri F, et al. Raman spectrum of graphene and graphene layers. Phys Rev Lett 2006;97(18):187401.
[40] Reina A, Jia X, Ho J, Nezich D, Son H, Bulovic V, et al. Layer area, few-layer graphene films on arbitrary substrates by chemical vapor deposition. Nano Lett 2009;9(8). 3087-3087.
[41] Chen T, Deng F, Zhu J, Chen C, Sun G, Ma S, et al. Hexagonal and cubic Ni nanocrystals grown on graphene: phase-controlled synthesis, characterization and their enhanced microwave absorption properties. J Mater Chem 2012;22(30):15190.
[42] Zhang M, Huang L, Chen J, Li C, Shi G. Ultrastrong, ultrastrong, and highly conductive graphene films with arbitrary sizes. Adv Mater 2014;26(45):7588–92.
[43] Li X, Zhang R, Yu W, Wang K, Wei J, Wu D, et al. Stretchable and highly sensitive graphene-on-polymer strain sensors. Sci Rep 2012;2:870.
[44] Zang X, Chen Q, Li P, He Y, Li X, Wang K, et al. Highly flexible and adaptable, all-solid-state supercapacitors based on graphene woven-fabric film electrodes. Small 2014;10(13):2583–8.
[45] Yang T, Wang Y, Li X, Zhang Y, Li X, Wang K, et al. Torsion sensors of high sensitivity and wide dynamic range based on a graphene woven structure. Nanoscale 2014;6(21):13053–9.
[46] Liu X, Sun X, Wang Z, Shen X, Wu Y, Kim JK. Planar porous graphene woven fabric/epoxy composites with exceptional electrical, mechanical properties, and fracture toughness. ACS Appl Mater Interfaces 2015;7(38):21455–64.
[47] Zhang Y, Zhang L, Zhou C. Review of chemical vapor deposition of graphene and related applications. Acc Chem Res 2013;46(10):2329–39.
[48] Chen CY, Dai D, Chen GX, Yu JX, Nishimura K, Lin CT, et al. Rapid growth of single-layer graphene on the insulating substrates by thermal CVD. Appl Surf Sci 2015;346:41–5.
[49] Parker WJ, Jenkins RJ, Butler CP, Abbott GL. Flash method of determining thermal diffusivity, heat capacity, and thermal conductivity. J Appl Phys 1961;32(9):1679.
[50] Tian X, Itkis ME, Bekyarova EB, Haddon RC. Anisotropic thermal and electrical properties of thin thermal interface layers of graphite nanoplatelet-based composites. Sci Rep 2013;3(4):1710.
[51] Koo M, Bae JS, Shim SE, Kim D, Nam D, Lee J, et al. Thermo-dependent characteristics of polyimide–graphene composites. Colloid Polym Sci 2011;289(13):1503–9.
[52] Zhang R, Chen Q, Zhen Z, Jiang X, Zhong M, Zhu H. Cellulose-templated graphene monoliths with anisotropic mechanical, thermal, and electrical properties. ACS Appl Mater Interfaces 2015;7(34):19145–52.
[53] Tseng IH, Chiang JC, Lin HC, Tsai MH. Polyimide/boron nitride nanocomposites. Chemistry 2012;70:31–8.
[54] Dai W, Yu J, Wang Y, Song Y, Bai H, Nishimura K, et al. Enhanced thermal and mechanical properties of polyimide/graphene composites. Macromol Res 2014;22(9):983–9.
[55] Yorifuji D, Ando S. Enhanced thermal conductivity over percolation threshold in polyimide blend films containing ZnO nano-pyramidal particles: advantage of vertical double percolation structure. J Mater Chem 2011;21(12):4402–7.
[56] Tseng I, Chang JC, Huang SL, Tsai MH. Enhanced thermal conductivity and dimensional stability of flexible polyimide nanocomposite film by addition of functionalized graphene oxide. Polym Int 2013;62(5):827–35.
[57] Dai W, Yu J, Wang Y, Song Y, Alam FE, Nishimura K, et al. Enhanced thermal conductivity for polyimide composites with a three-dimensional silicon carbide nanowire@graphene sheets filler. J Mater Chem A 2015;3(9):4884–91.
[58] Ding P, Zhang J, Song N, Tang S, Liu Y, Shi L. Anisotropic thermal conductive properties of hot-pressed polystyrene/graphene composites in the through-plane and in-plane directions. Compos Sci Technol 2015;109:25–31.